Artif Life Robotics (2017) 22:175–183
DOI 10.1007/s10015-017-0349-2

ORIGINAL ARTICLE

Modeling of humanoid dynamics including slipping with nonlinear floor friction

Xiang Li[1] · Hiroki Imanishi[1] · Mamoru Minami[1] · Takayuki Matsuno[1] · Yanou Akira[1]

Received: 7 April 2016 / Accepted: 18 December 2016 / Published online: 4 February 2017

Abstract Biped locomotion created by controlling methods based on zero-moment point has been realized in real world and been well verified its efficacy for stable walking. However, the walking strategies that have been proposed so far seems to avoid such considerations as slipping of foot on the floor, even though there should exist the slipping large or small in real world. In this research, a dynamical model of humanoid robot including slipping of foot is proposed, which is derived by the Newton–Euler method. To confirm the veracity of the derived dynamical model, the model has been verified from the view point that when all friction coefficients are identical to zero, the total kinetic energy should be conserved to be unchanged, and when the coefficients are not zero, the total kinetic energy should decrease monotonously.

Keywords Humanoid · Slipping · Friction · Bipedal · Dynamical · Newton–Euler Method

1 Introduction

Human beings have acquired an ability of stable bipedal walking in evolving so far in a repetition of generation. From a view point of making a stable controller for the bipedal walking based on knowledge of control theory, it looks not easy because of the complicated dynamics with high nonlinearity and coupled interactions between state variables with high dimensions. Therefore, how to simplify the complicated walking dynamics to help construct stable walking controller has been studied intensively.

Avoiding complications in dealing directly with true dynamics without approximation, inverted pendulum has been used frequently for making a controller [1–3], using the merits to simplify the calculations to determine control input torque. Furthermore, linear approximation that makes the humanoid model represented by simple inverted pendulum enables researchers to realize stable gait through well-known control strategy [4–6], since these researches include assumptions justifying the approximations, the hypotheses leaves obscureness in the discussions of the robot's dynamical behaviors.

Our research has begun from similar view point of [7, 8] as aiming to describe gait's dynamics as correctly as possible, including slipping of foot on the floor, with whole body humanoid dynamics consisted of head, waist, torso, arms and legs. Importantly, the authors think that the dimension of dynamical equation will change depending on the walking gait's varieties which has been discussed in [9] using one legged hopping robot. In fact, this kind of dynamics with the dimension number of state variables varying by the result of its dynamical time transitions are out of the arena of control theory that discusses how to control a system with fixed states' number. Furthermore, the tipping over motion has been called as nonholonomic dynamics that includes a joint without inputting torque, i.e., free joint that is rotation of toe when walking and especially stumbling. Landing of the heel or the toe of lifting leg in the air to the ground makes a geometrical contact [10] and the contact gives a constraint condition to the humanoid's dynamics.

This work was presented in part at the 21st International Symposium on Artificial Life and Robotics, Beppu, Oita, January 20–22, 2016.

✉ Xiang Li
pzkm87r2@s.okayama-u.ac.jp

[1] Okayama, Japan

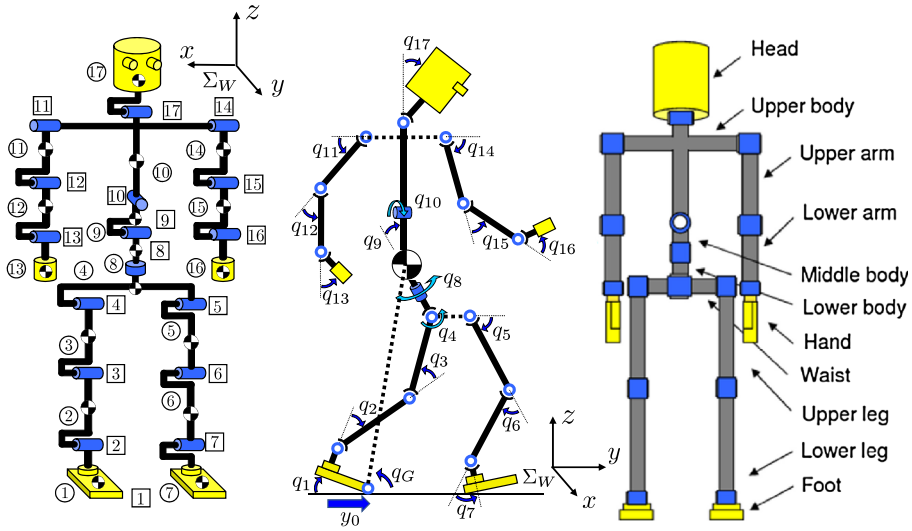

Fig. 1 Definition of humanoid's link, joint and whole body

The conventional NE method could be applied only to a robot having an open loop serial linkage structure, therefore, the dynamical model of robots made by NE method was limited within a condition that the robot does not contact external world. Therefore, the NE method has not been utilized for modeling of robots that works under a premise that it contacts with the environment, e.g., when the robot conducts some grinding task or assembling task. To eliminate this limitation, one of the author has proposed Extended NE (ENE) method [11] that could be utilized for dynamical modeling of manipulator whose hand is kinematically constraint by non-elastic environment. This method utilizes recursive calculation of acceleration and exerting force/torque along to the robot's serial link structure including inner force/torque and that this is important merit of the ENE that Lagrange method does not have. The demerit of ENE is that the constraint force exerting between the robot and the environment should be predetermined before recursive calculation starts. Averting the demerit of the ENE, it is convenient to deal with the constraint motion problem by solving robot's angular acceleration and contacting force through simultaneous equation, which has been introduced by [12] and published in a book [13]. Then the simultaneous solving method [13] of the acceleration and contacting force has been used for describing the humanoid's walking dynamics with contacting constraints over the external environments, which is in this paper, the floor on which the humanoid walks.

In this research that is based on [14, 15], a walking model of humanoid robot including slipping, bumping, surface-contacting and point-contacting of foot is discussed, and its dynamical equation is derived by the NE method. Especially the common consideration of the free-leg model [16–18] is without any slipping. Additionally, this research is different from the previous humanoid researches [19–22], that the nonlinear friction which includes the static/kinetic friction will be discussed in walking model of humanoid robot consisting of 17 rigid links. [19, 20] are the experimental discussions on walking with slippage. And [21, 22] have tried to discuss the influences of stick/slip slipping states during walking, however, those papers lack description of relations between full body dynamical model and the stick/slip states of foot.

In this paper, a dynamical model of humanoid including influences of nonlinearity caused by stick-slip [23–25] motions, which are derived from the nonlinear friction between the floor and humanoid's feet, will be introduced.

Table 1 Physical parameters

Link	l_i (m)	m_i (kg)	d_i (N ms/rad)
Head	0.24	4.5	0.5
Upper body	0.41	21.5	10.0
Middle body	0.1	2.0	10.0
Lower body	0.1	2.0	10.0
Upper arm	0.31	2.3	0.03
Lower arm	0.24	1.4	1.0
Hand	0.18	0.4	2.0
Waist	0.27	2.0	10.0
Upper leg	0.38	7.3	10.0
Lower leg	0.40	3.4	10.0
Foot	0.07	1.3	10.0
Total weight (kg)	–	64.2	–
Total hight (m)	1.7	–	–

2 Dynamical walking model

2.1 Forward kinematical calculations

We discuss a biped robot whose definition is depicted in Fig. 1. Table 1 indicates length l_i (m), mass m_i (kg) of links and coefficient of joints' viscous friction d_i (N m s/rad), which are decided based on [26]. This model is simulated as a serial-link manipulator having ramifications and represents rigid whole body—feet including toe, torso, arms and so on—by 17 degree-of-freedom. Though motion of legs is restricted in sagittal plane, it generates varieties of walking gait sequences since the robot has flat-sole feet and kicking torque. In this paper, one foot including link-1 is defined as "supporting-leg" and another foot including link-7 is defined as "free-leg" ("contacting-leg" when the free-leg contacts with floor) according to the walking state.

In this paper, we derive the equation of motion following by NE formulation [22, 23]. So we must consider the structure of the supporting-leg with two situations. When the supporting-leg is constituted by rotating joint: we first have to calculate relations of positions, velocities and accelerations between links as forward kinetics procedures from bottom link to top link. Serial link's angular velocity ${}^i\boldsymbol{\omega}_i$, angular acceleration ${}^i\dot{\boldsymbol{\omega}}_i$, acceleration of the origin ${}^i\ddot{\boldsymbol{p}}_i$ and acceleration of the center of mass ${}^i\ddot{\boldsymbol{s}}_i$ based on Σ_i fixed at ith link are obtained as follows.

$$ {}^i\boldsymbol{\omega}_i = {}^{i-1}\boldsymbol{R}_i^T\, {}^{i-1}\boldsymbol{\omega}_{i-1} + \boldsymbol{e}_{z_i}\dot{q}_i \tag{1} $$

$$ {}^i\dot{\boldsymbol{\omega}}_i = {}^{i-1}\boldsymbol{R}_i^T\, {}^{i-1}\dot{\boldsymbol{\omega}}_{i-1} + \boldsymbol{e}_z\ddot{q}_i + {}^i\boldsymbol{\omega}_i \times (\boldsymbol{e}_{z_i}\dot{q}_i) \tag{2} $$

$$ \begin{aligned} {}^i\ddot{\boldsymbol{p}}_i = {}& {}^{i-1}\boldsymbol{R}_i^T\{{}^{i-1}\ddot{\boldsymbol{p}}_{i-1} + {}^{i-1}\dot{\boldsymbol{\omega}}_{i-1} \times {}^{i-1}\hat{\boldsymbol{p}}_i \\ & + {}^{i-1}\boldsymbol{\omega}_{i-1} \times ({}^{i-1}\boldsymbol{\omega}_{i-1} \times {}^{i-1}\hat{\boldsymbol{p}}_i)\} \end{aligned} \tag{3} $$

$$ {}^i\ddot{\boldsymbol{s}}_i = {}^i\ddot{\boldsymbol{p}}_i + {}^i\dot{\boldsymbol{\omega}}_i \times {}^i\hat{\boldsymbol{s}}_i + {}^i\boldsymbol{\omega}_i \times ({}^i\boldsymbol{\omega}_i \times {}^i\hat{\boldsymbol{s}}_i) \tag{4} $$

Then if the supporting-leg is constituted by prismatic joint. We will switch the equations as the following.

$$ {}^i\boldsymbol{\omega}_i = {}^{i-1}\boldsymbol{R}_i^{\mathrm{T}}\, {}^{i-1}\boldsymbol{\omega}_{i-1} \tag{5} $$

$$ {}^i\dot{\boldsymbol{\omega}}_i = {}^{i-1}\boldsymbol{R}_i^{\mathrm{T}}\, {}^{i-1}\dot{\boldsymbol{\omega}}_{i-1} \tag{6} $$

$$ \begin{aligned} {}^i\ddot{\boldsymbol{p}}_i = {}& {}^{i-1}\boldsymbol{R}_i^{\mathrm{T}}\{{}^{i-1}\ddot{\boldsymbol{p}}_{i-1} + {}^{i-1}\dot{\boldsymbol{\omega}}_{i-1} \times {}^{i-1}\hat{\boldsymbol{p}}_i \\ & + {}^{i-1}\boldsymbol{\omega}_{i-1} \times ({}^{i-1}\boldsymbol{\omega}_{i-1} \times {}^{i-1}\hat{\boldsymbol{p}}_i)\} \\ & + 2({}^{i-1}\boldsymbol{R}_i^{Ti-1}\boldsymbol{\omega}_{i-1}) \times (\boldsymbol{e}_z\dot{q}_i) + \boldsymbol{e}_z\ddot{q}_i \end{aligned} \tag{7} $$

$$ {}^i\ddot{\boldsymbol{s}}_i = {}^i\ddot{\boldsymbol{p}}_i + {}^i\dot{\boldsymbol{\omega}}_i \times {}^i\hat{\boldsymbol{s}}_i + {}^i\boldsymbol{\omega}_i \times ({}^i\boldsymbol{\omega}_i \times {}^i\hat{\boldsymbol{s}}_i) \tag{8} $$

here, ${}^{i-1}\boldsymbol{R}_i$ means orientation matrix, ${}^{i-1}\hat{\boldsymbol{p}}_i$ represents position vector from the origin of $(i-1)$th link to the one of ith, ${}^i\hat{\boldsymbol{s}}_i$ is defined as gravity center position of ith link and $\boldsymbol{e}_{z_i}$ is unit vector that shows rotational axis of ith link. However, velocity and acceleration of 4th link transmit to 8th link and ones of 10th link transmit to 11th, 14th and 17th link directly because of ramification mechanisms.

2.2 Backward inverse dynamical calculations

After the above forward kinetic calculation has been done, contrarily inverse dynamical calculation from top to base link are shown as follow. Newton equation and Euler equation of i-th link are represented by Eqs. (9), (10) when ${}^i\boldsymbol{I}_i$ is defined as inertia tensor of ith link. Here, ${}^i\boldsymbol{f}_i$ and ${}^i\boldsymbol{n}_i$ in Σ_i show the force and moment exerted on ith link from i+1th link.

$$ {}^i\boldsymbol{f}_i = {}^i\boldsymbol{R}_{i+1}\, {}^{i+1}\boldsymbol{f}_{i+1} + m_i{}^i\ddot{\boldsymbol{s}}_i \tag{9} $$

$$ \begin{aligned} {}^i\boldsymbol{n}_i = {}& {}^i\boldsymbol{R}_{i+1}\, {}^{i+1}\boldsymbol{f}_{i+1} + {}^i\boldsymbol{I}_i{}^i\dot{\boldsymbol{\omega}}_i + {}^i\boldsymbol{\omega}_i \times ({}^i\boldsymbol{I}_i{}^i\boldsymbol{\omega}_i) \\ & + {}^i\hat{\boldsymbol{s}}_i \times (m_i{}^i\ddot{\boldsymbol{s}}_i) + {}^i\hat{\boldsymbol{p}}_{i+1} \times ({}^i\boldsymbol{R}_{i+1}\, {}^{i+1}\boldsymbol{f}_{i+1}) \end{aligned} \tag{10} $$

On the other hand, since force and torque of 5th and 8th links are exerted on 4th link, effects onto 4th link as:

$$ {}^4\boldsymbol{f}_4 = {}^4\boldsymbol{R}_5{}^5\boldsymbol{f}_5 + {}^4\boldsymbol{R}_8{}^8\boldsymbol{f}_8 + m_4{}^4\ddot{\boldsymbol{s}}_4, \tag{11} $$

$$ \begin{aligned} {}^4\boldsymbol{n}_4 = {}& {}^4\boldsymbol{R}_5{}^5\boldsymbol{n}_5 + {}^4\boldsymbol{R}_8{}^8\boldsymbol{n}_8 + {}^4\boldsymbol{I}_4{}^4\dot{\boldsymbol{\omega}}_4 + {}^4\boldsymbol{\omega}_4 \times ({}^4\boldsymbol{I}_4{}^4\boldsymbol{\omega}_4) \\ & + {}^4\hat{\boldsymbol{s}}_4 \times (m_4{}^4\ddot{\boldsymbol{s}}_4) + {}^4\hat{\boldsymbol{p}}_5 \times ({}^4\boldsymbol{R}_5{}^5\boldsymbol{f}_5) \\ & + {}^4\hat{\boldsymbol{p}}_8 \times ({}^4\boldsymbol{R}_8{}^8\boldsymbol{f}_8). \end{aligned} \tag{12} $$

Similarly, force and torque of 11th, 14th and 17th links transmit to 10th link directly. Then, rotational motion equation of ith link is obtained as Eq. (13) by making inner product of induced torque onto the ith link's unit vector $\boldsymbol{e}_{z_i}$ around rotational axis:

$$ \tau_i = \boldsymbol{e}_{z_i}^T\, {}^i\boldsymbol{n}_i + d_i\dot{q}_i. \tag{13} $$

However, when the supporting-leg (1st link) slipping (prismatic joint), the torque onto the 1st link can be calculated by following equation.

$$ f_1 = \boldsymbol{e}_{z_1}^T\, {}^1\boldsymbol{f}_1 + \mu_k\dot{y}_0. \tag{14} $$

Finally, we get motion equation with one leg standing as:

$$ \boldsymbol{M}(\boldsymbol{q})\ddot{\boldsymbol{q}} + \boldsymbol{h}(\boldsymbol{q}, \dot{\boldsymbol{q}}) + \boldsymbol{g}(\boldsymbol{q}) + \boldsymbol{D}\dot{\boldsymbol{q}} = \boldsymbol{\tau}, \tag{15} $$

here, $\boldsymbol{\tau} = [f_1, \tau_1, \tau_2, \ldots, \tau_{17}]$ is input torque, $\boldsymbol{M}(\boldsymbol{q})$ is inertia matrix, both of $\boldsymbol{h}(\boldsymbol{q}, \dot{\boldsymbol{q}})$ and $\boldsymbol{g}(\boldsymbol{q})$ are vectors which indicate Coriolis force, centrifugal force and gravity. When the

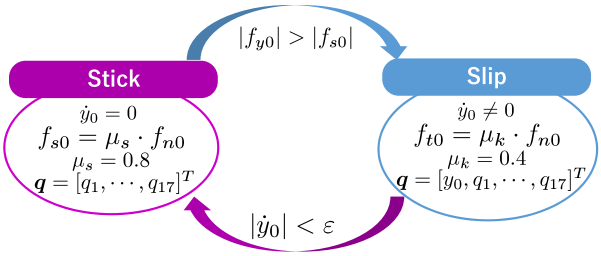

Fig. 2 Switch conditions of stick-slip motion

supporting-leg slipping, the $\boldsymbol{D} = \mathrm{diag}[\mu_k, d_1, d_2, \ldots, d_{17}]$ is a matrix which means coefficients of joints and between foot and ground. And $\boldsymbol{q} = [y_0, q_1, q_2, \ldots, q_{17}]^T$ means the angle of joints and the relative position between foot and ground. When the supporting-leg slipping, the variable vector $\boldsymbol{q}$ consists of $\boldsymbol{q} = [y_0, q_1, q_2, \ldots, q_{17}]^T$. The viscous friction of y-axis (slipping axis) can be described as $\mu_k \dot{y}_0$ that is included in left-side of Eq. (15), and the nonlinear force generated by reaction force to the supporting-leg f_{t0} is made by $f_{t0} = \mu_k f_{n0}$ where f_{n0} is normal force exerting to supporting-leg caused by dynamical coupling of the humanoid body given by Eqs. (9) and (10), and μ_k is dynamical friction coefficient.

This slipping motion state is depicted at right side of Fig. 2. If $|\dot{y}_0| < \epsilon$ is satisfied, then the degree of motion, y_0 , disappears, then the equation of motion transfers to the equation of motion that consists of $\boldsymbol{q} = [q_1, q_2, \ldots, q_{17}]^T$. On this state, static friction coefficient $\mu_s = 0.8$ is applied, and static friction force $f_{s0} = \mu_s f_{n0}$ exerts to the lateral direction of foot. when the exerting lateral force f_{y0} generated by dynamical coupling of humanoid body, that is ${}^i\boldsymbol{n}_i$ in Eq. (13) should satisfy $|f_{y0}| > |f_{s0}|$, then the slipping motion starts and the equation of motion, Eq. (15), is changed into the one with variables of $\boldsymbol{q} = [y_0, q_1, q_2, \ldots, q_{17}]^T$ again, which is depicted at the right state Fig. 2.

3 Validation of model

3.1 Verification by mechanical energy

To verify this complex model, we use the mechanical energy conservation law. Because to verify the conservation of mechanical energy, the equation of motion must be correct. We make the model to do a free fall with the input torque $\boldsymbol{\tau}_i = 0$ and the viscous friction $\boldsymbol{D}_i = 0$. In this case, there is no friction. So, it will have no discharge of energy during free fall. During the motion the mechanical energy will be saved at the initial potential energy. To derive the mechanical energy, it is necessary to calculate all of the potential energy, rotational energy and translational energy.

3.2 Calculation of mechanical energy

It is necessary to calculate the height of the center of gravity of each link before the calculation of the potential energy. We use the homogeneous transformation matrix to calculate it as following equation.

$$ {}^W z_{Gi} = {}^W z_i + \frac{{}^W z_{i+1} - {}^W z_i}{2} \tag{16} $$

here, ${}^W z_{Gi}$ means the height of C.o.G of ith link in world coordinate system ${}^W z_i$ is the height of the joint which is seen from the world coordinate. So, we can calculate the potential energy as following equation.

$$ E_p = \sum_{i=1}^{17} m_i {}^W z_i g \tag{17} $$

here, E_p is the potential energy of the model. m_i is the mass of each link. g is the gravitational acceleration. Then, we can calculate the rotational energy as following equation.

$$ E_k = \sum_{i=1}^{17} \frac{1}{2} {}^W \boldsymbol{\omega}_i^T {}^W \boldsymbol{I}_i {}^W \boldsymbol{\omega}_i \tag{18} $$

Here, E_k is the rotational energy of the model. $\boldsymbol{I}_i$ is the moment of inertia of each link. Then, we can also calculate the translational energy as following equation.

$$ E_v = \sum_{i=1}^{17} \frac{1}{2} m_i {}^W \dot{\boldsymbol{r}}_{gi}^T {}^W \dot{\boldsymbol{r}}_{gi} \tag{19} $$

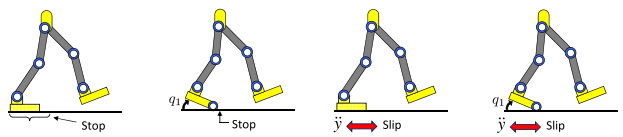

(a) Supporting-foot surface contact (stop) **(b)** Supporting-foot line contact (stop) **(c)** Supporting-foot surface contact (slip) **(d)** Supporting-foot line contact (slip)

Fig. 3 Ground state of the supporting-foot

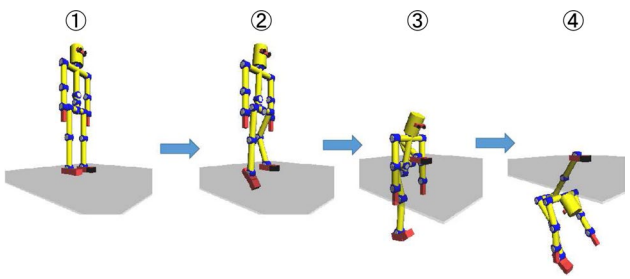

Fig. 4 Free-fall of humanoid model with the supporting-foot in the state of rest

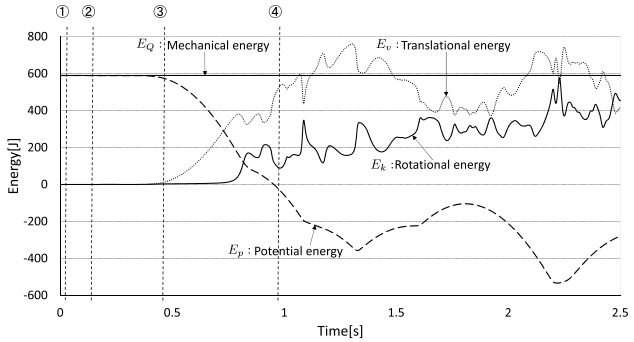

Fig. 5 Mechanical energy conservation during the supporting-foot in the stopped and surface contact state (Fig. 3a)

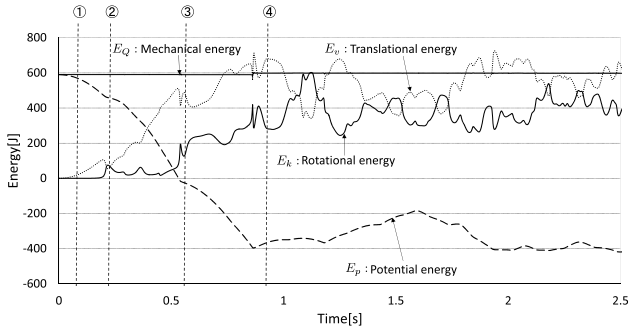

Fig. 6 Mechanical energy conservation during the supporting-foot in the stopped and line contact state (Fig. 3b)

Here, E_v is the translational energy of the model, $\dot{\boldsymbol{r}}_{gi}$ is the translational velocity of C.o.G of i-th link. Finally, the mechanical energy can be derived as following equation.

$$E_Q = E_p + E_k + E_v \tag{20}$$

3.3 Verification simulation experiment

First, the model for a humanoid whose supporting-foot is at rest with surface contact is shown in Fig. 3a. On that assumption of foot contacting condition in Fig. 3a, free falling simulation has been done as shown in Fig. 4①–④. With the condition of viscous friction (D_i=0) and input torque ($\boldsymbol{\tau} = \mathbf{0}$). Fig. 5 shows the result of the mechanical energy when the supporting-foot stops with surface contact state. The mechanical energy E_Q keeps constant even though translation energy E_v, rotational energy E_k and potential energy E_p fluctuate widely during free fall motions depicted in Fig. 4①–④. And Fig. 6 is the simulated result of same condition except that the supporting-foot contacts in a line with floor with the toe as shown in Fig. 3b. From Figs. 5 and 6, E_Q can be seen constant. So, it shows that the model with support-foot stopped has no contradictions.

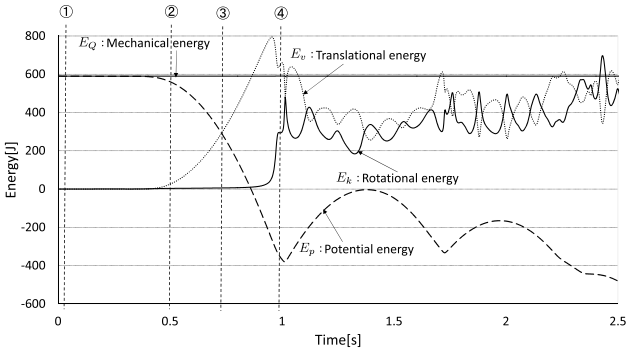

Fig. 7 Mechanical energy conservation during the supporting-foot in the slip and surface contact state (Fig. 3c)

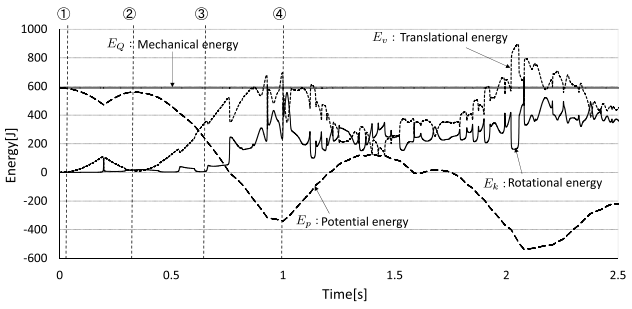

Fig. 8 Mechanical energy conservation during the supporting-foot in the slip and line contact state (Fig. 3d)

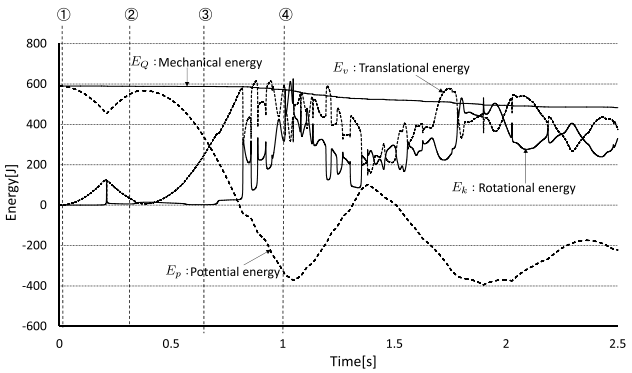

Fig. 9 Mechanical energy discharging during the supporting-foot in the slip and line contact state (Fig. 3d) and with sliding friction coefficient 0.5

Similarly, the simulation about the slip state of the supporting-foot with surface contact and line contact are shown in Fig. 3c, d. As well as Fig. 4, the humanoid models are also examined by a free fall without any viscous friction and input torque. Fig. 7 shows the result of E_Q when the

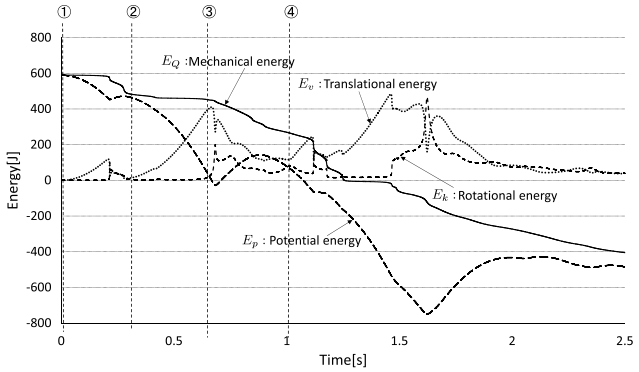

Fig. 10 Mechanical energy discharging during the supporting-foot in the slip and line contact state (Fig. 3d) with sliding friction coefficient 0.5 and viscous friction coefficient $D_i = 0.2$ in all of rotational joints

supporting-foot is in the slip and surface contact state. And Fig. 8 is about E_Q during the supporting-foot is in the slip and line contact state. From Figs. 7 and 8, the total mechanical energy can be seen constant.

Figure 9 also shows a free-fall with the same condition of Fig. 8 (Fig. 3d) and the sliding friction coefficient of ground is set to 0.5 to have the energy reducing influence explicit. It can be seen that in the case of Fig. 9, E_Q discharged by the friction and the decreasing profile is monotonous as expected. Furthermore, Fig. 10 shows a simulation that is based of Fig. 9, adding the viscous friction coefficient $D_i = 0.2$ to all rotational joints, and keep the other conditions of Fig. 9. It can also be seen that in the case of Fig. 10, the mechanical energy E_Q discharged by both sliding and viscous friction, the discharging speed is faster than the case with sliding friction only shown in Fig. 9.

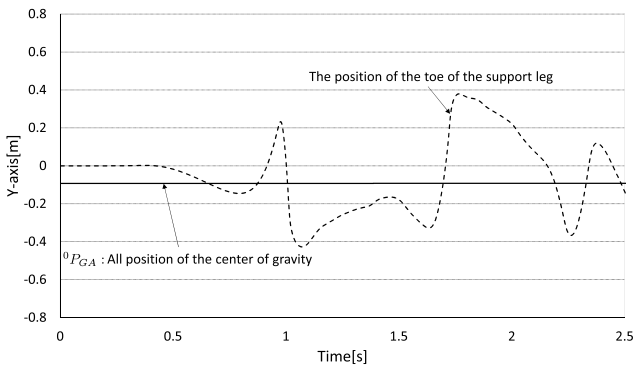

Fig. 11 The y-position of the overall center of gravity during the supporting-foot in the slip and surface contact state (Fig. 3c)

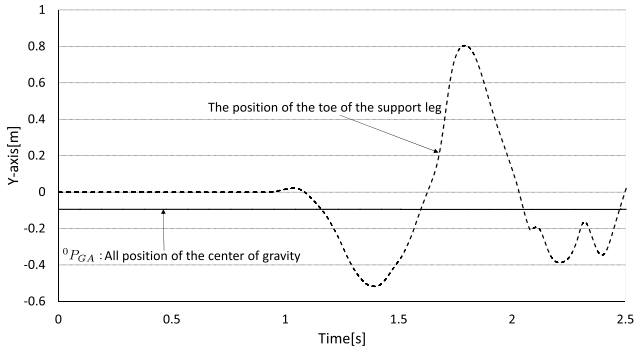

Fig. 12 The y-position of the overall center of gravity during the supporting-foot in the slip and line contact state (Fig. 3d)

3.4 Verification by the position of the overall center of gravity

In the simulation of free fall, if the supporting-foot can slip on the ground (without any friction), the y-position of Σ_0 (Σ_0 is defined in Fig. 1) of the overall center of gravity ${}^0P_{GA}$ should not change. To confirm that, the y-position of the overall center of gravity is given by following equation.

$$ {}^0P_{GA} = \frac{\sum_{i=1}^{17} m_i {}^0P_{Gi}}{\sum_{i=1}^{17} m_i} \tag{21} $$

Here, ${}^0P_{Gi}$ is the y-position of center of gravity of each link.

The ${}^0P_{GA}$ during free fall simulation that is supporting-foot in slip surface contact state and slip line contact state are shown in Figs. 11 and 12. From Figs. 11 and 12, the y-position of the overall center of gravity is not changed even though the toe position of the supporting-foot fluctuate in time domain. So, there is no contradiction against common sense.

3.5 Simulation including stick-slip

Another simulation with nonlinear friction between floor and foot has been prepared to examine a stick-slip motion that can verify the humanoid model further. The experiment conditions are shown as follows. The state (stick or slip) of supporting-leg that is dominated by the stick-slip conditions are shown in Fig. 2. When the driving force exerting to supporting-leg from dynamical coupling of humanoid nonlinear model f_{y0} is larger than the maximum static frictional force f_{s0}, the supporting-leg starts to slip. Here f_{n0} means the normal force exerting to the foot, and when the slip velocity of supporting-leg $|\dot{y}_0|$ is less than ϵ (a very small value $\epsilon = 0.001$ (m/s) $= 1$ (mm/s) in this paper), the supporting-leg enters a stick state. During the supporting-leg in stick state, the coefficient of friction is set to $\mu_s = 0.8$, and when the supporting-leg is in slip state,

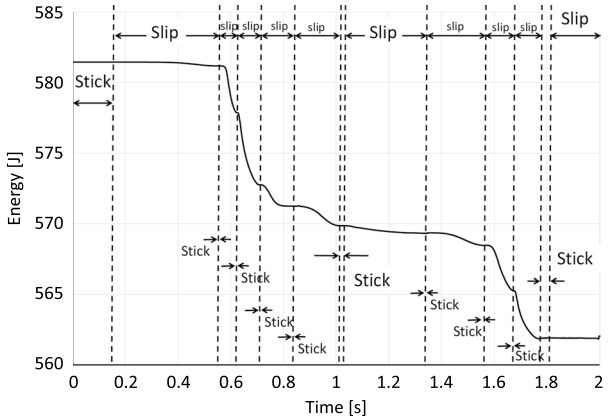

Fig. 13 Mechanical energy

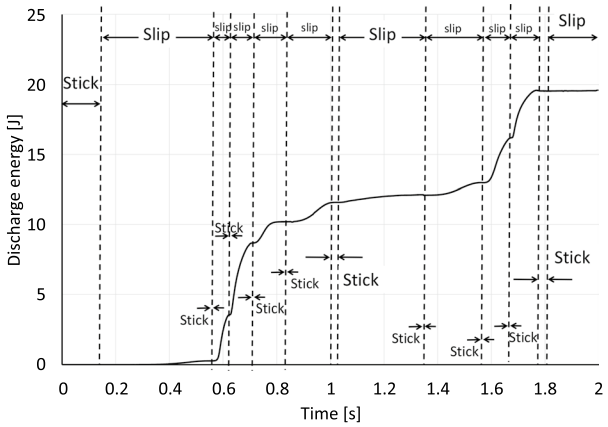

Fig. 14 Discharge of energy by friction

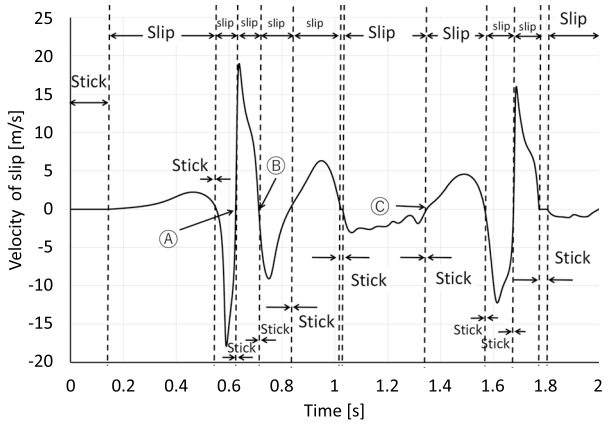

Fig. 15 Velocity of slip

the coefficient is set to $\mu_k = 0.4$. And the body of humanoid robot will fall freely without any viscous friction ($\boldsymbol{D} = \boldsymbol{0}$) and input torque ($\boldsymbol{\tau} = \boldsymbol{0}$).

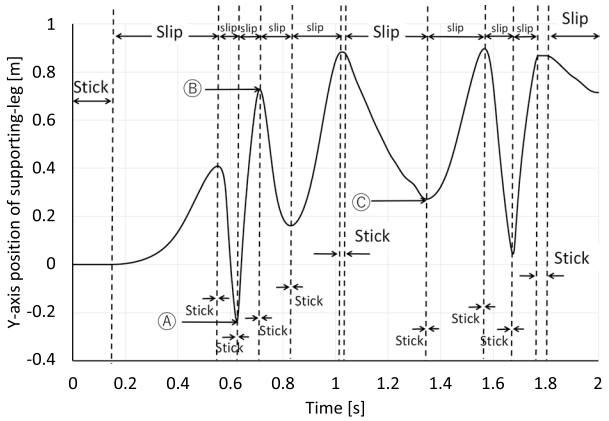

Fig. 16 y-position of supporting-leg

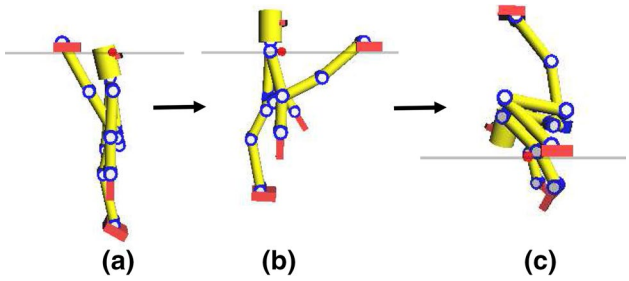

Fig. 17 Configurations during free-fall simulation shown in Fig. 16, **a** the configuration at time Ⓐ designated in Fig. 16, and **b**, **c** corresponds to time Ⓑ and Ⓒ

$$E_{\text{discharge}} = \int_0^t \mu_k \dot{y}_0^2 \mathrm{d}t \tag{22}$$

Figure 13 shows time profile of mechanical energy of humanoid's free-fall motion including the stick-slip motion, and Fig. 14 shows the discharged energy caused by friction on floor, the calculation of discharged energy is shown in Eq. (22). Here, μ_k means the coefficient of friction when slipping, and when sticking the $E_{\text{discharge}}$ in Eq. (22) equal to zero since $\dot{y}_0$ is zero. In Figs. 13 and 14, when the supporting-leg is in the state of stick, the total mechanical energy is remained unchanged. And the mechanical energy discharges while the supporting-leg slipping, and the value of discharged energy in Fig. 14 is consistent with the result in Fig. 13.

Furthermore, the velocity and the y-axis position of supporting-leg are shown in Figs. 15 and 16. Figure 15 shows that when the supporting-leg is in the state of stick, the velocity of slip equals to zero, and Fig. 16 shows that the y-axis position is also not changed in time. And the discharge of energy depends on the velocity of slip. When the supporting-leg slipping is faster, the discharge of energy also gets a higher rate. Conversely, when the supporting-leg slipping is very slow or stops, the discharge of energy

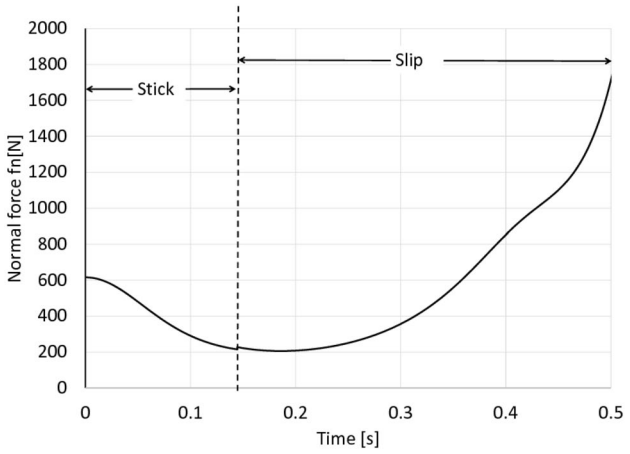

Fig. 18 Normal force f_n during stick-slip motion

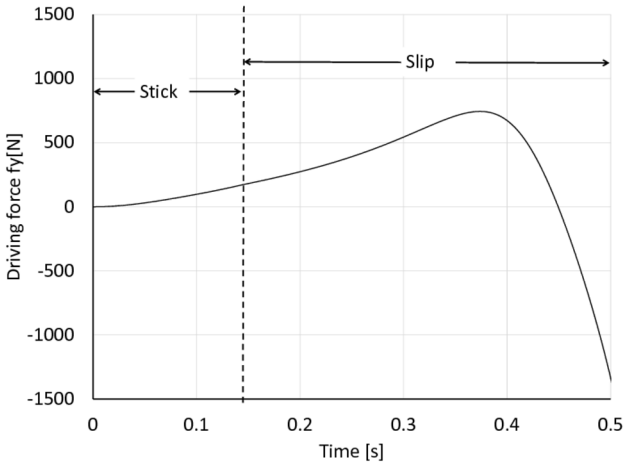

Fig. 19 Diving force f_y of slipping direction

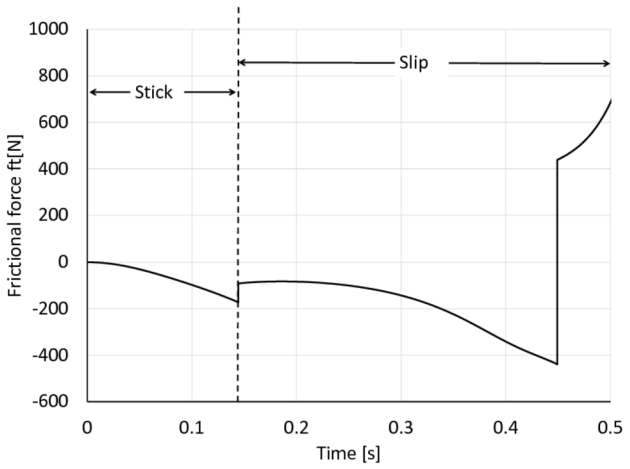

Fig. 20 Friction f_t between foot and floor

is also small or kept unchanged. So, from this simulation, it can also be seen that supporting-leg slip-stick model is feasible.

Figure 17 shows their shapes of the humanoid while the simulated motion proceeds as shown in Figs. 13 , 14, 15 and 16. The configuration in Fig. 17a was detected at the time designated by A in Figs. 15 and 16, and also b, c are the shapes at B and C in the both figures.

Furthermore, the normal force f_n, diving force f_y of slipping direction (right is the plus direction) and friction f_t between foot and floor are shown in Figs. 18, 19 and 20. During the free-fall simulation, the normal force becomes smaller and the diving force becomes bigger at the first stick state. At the moment, the friction f_t is not decided by the normal force, the value of f_t is equal to f_y (but f_t is always in the opposite direction of f_y). When supporting-leg starts to slip, the coefficient of friction also switch to $\mu_k = 0.4$. At the moment, the friction becomes smaller and the friction is directly proportional to the normal force. So, from this simulation, it can also be seen that supporting-leg slip-stick model is feasible.

4 Conclusion

In this paper, a dynamical model of humanoid robot including slipping of foot is proposed, the equation of motion is derived by Newton–Euler method. And the model has been verified using the mechanical energy-conservation law. For the future, the authors plan to extend the calculation method to the case of more than two constraint conditions, and evaluate it by simulations.

References

1. Kajita S, Morisawa M, Miura K, Nakaoka S, Harada K, Kaneko K, Kanehiro F, Yokoi K (2010) Biped walking stabilization based on linear inverted pendulum tracking. In: Proceedings of IEEE/RSJ international conference on intelligent robots and systems, pp 4489–4496
2. Dau H, Chew C, Poo A (2010) Proposal of augmented linear inverted pendulum model for bipedal gait planning. In: Proceedings of IEEE/RSJ international conference on intelligent robots and systems, pp 172–177
3. Park JH, Kim KD (1998) Biped walking robot using gravity-compensated inverted pendulum mode and computed torque control. Proc IEEE Int Conf Robot Autom 4:3528–3593
4. Wieber PB (2006) Trajectory free linear model predictive control for stable walking in the presence of strong perturbations. In: Proceedings of international conference on humanoid robotics
5. Wieber PB (2008) Viability and predictive control for safe locomotion. In: Proceedings of IEEE/RSJ international conference on intelligent robots and systems
6. Herdt A, Perrin N, Wieber PB (2010) Walking without thinking about it. In: Proceedings of IEEE/RSJ international conference on intelligent robots and systems, pp 190–195

7. Huang Y, Chen B, Wang Q, Wei K, Wang L (2010) Energetic efficiency and stability of dynamic bipedal walking gaits with different step lengths. In: Proceedings of IEEE/RSJ international conference on intelligent robots and systems, pp 4077–4082
8. Sobotka M, Buss M (2005) A hybrid mechatronic tiliting robot: modeling, trajectories, and control. In: Proceedings of the 16th IFAC world congress
9. Wu T, Yeh T, Hsu B (2010) Trajectory planning of a one-legged robot performing stable hop. In: Proceedings of IEEE/RSJ international conference on intelligent robots and systems, pp 4922–4927
10. Nakamura Y, Yamane K (2000) Dynamics of kinematic chains with discontinuous changes of constraints—application to human figures that move in contact with the environments. J RSJ 18(3):435–443 (in Japanese)
11. Nishiguchi J, Minami M, Yanou A (2014) Iterative calculation method for constraint motion by extended Newton–Euler method and application for forward dynamics. Trans JSME 80(815)
12. Hemami H, Wyman BF (1979) Modeling and control of constrained dynamic systems with application to biped locomotion in the frontal plane. IEEE Trans Autom Control AC–24–4:526–535
13. Siciliano B, Khatib O (2008) Handbook of robotics. Section kinematic loops. Springer, Berlin
14. Feng T, Nishiguchi J, Li X, Minami M, Yanou A, Matsuno T (2015) Dynamical analyses of humanoid's walking by using extended Newton–Euler method. 20st international symposium on artificial life and robotics (AROB 20st)
15. Kobayashi Y, Minami M, Yanou A, Maeba T (2013) Dynamic reconfiguration manipulability analyses of humanoid bipedal walking. IEEE international conference on robotics and automation (ICRA), pp 4764–4769
16. Aoyama T, Hasegawa Y, Sekiyama K, Fukuda T (2009) Stabilizing and direction control of efficient 3-D biped walking based on PDAC. 2009 IEEE/ASME transactions on mechatronics, pp 712–718
17. Sugihara T, Nakamura Y (2003) Whole-body cooperative COG control through ZMP manipulation for humanoid robots. In: Proceedings of the 2nd international symposium on adaptive motion of animals and machines, SaP-III-4
18. Chevallereau C, Grizzle JW, Shih C-L (2009) Asymptotically stable walking of a five-link underactuated 3-D bipedal robot. IEEE transactions on robotics, vol 25, No. 1
19. Kajita S, Kaneko K, Harada K, Kanehiro F, Fujiwara K, Hirukawa H (2004) Biped walking on a low friction floor. In: Proceedings of the IEEE/RSJ international conference on intelligent robots and systems, pp 3546–3552
20. Kaneko K, Kanehiro F, Kajita S, Morisawa M, Fujiwara K, Harada K, Hirukawa H (2005) Slip observer for walking on a low friction floor. In: Proceedings of the IEEE/RSJ international conference on intelligent robots and systems, pp 634–640
21. Boone GN, Hodgins JK (1997) Slipping and tripping reflexes for bipedal robots. Auton Robots 4:259–271
22. Park JH, Kwon O (2001) Reflex control of biped robot locomotion on a slippery surface. In: Proceedings of the IEEE international conference on robotics and automation, pp 4134–4139
23. Ueda Y, Henmi M (1996) An experimental and analytical study on stick-slip motions. Technical report of lEICE, CAS vol 96, pp 41–48
24. Tokashiki LR, Fujita T, Kagawa T (1999) Stick-slip motion in pneumatic cylinders driven by meter-out circuit 1st report, friction characteristics and stick-slip motion. Trans Jpn Hydraul Pneum Soc 30(4):110–117
25. Nakano K (2007) A guideline of machinary design for preventing stick-slip. Nippon Gomu Kyokaishi 80(4):134–139
26. Kouchi M, Mochimaru M, Iwasawa H, Mitani S (2000) Anthropometric database for Japanese Population 1997–98. Japanese Industrial Standards Center, AIST, MITI